Unraveling the roGFP2 Cu(I) Sensing Mechanism

Alex M. Maldonado
Department of Biological Sciences
University of Pittsburgh
Pennsylvania, United States
alex.maldonado@pitt.edu

Here, we propose an atomistic mechanism for Cu(I) sensing for a redox-sensitive green fluorescent protein variant, roGFP2. **TODO: This is a very rough draft and not polished. Ideas and concepts are stable.**

1. GFP fluorescence mechanism

The fluorescence mechanism in green fluorescent protein (GFP) is a complex interplay of photophysical and photochemical processes that occur at the molecular level. This section delves into the current understanding of fluorescence in GFP, exploring the fundamental principles of excitation and de-excitation, as well as the various factors that influence these processes. We will examine how the protein environment modulates the fluorescent properties, the critical role of chromophore protonation states, and the intricate dynamics of excited-state phenomena such as non-adiabatic crossings and proton transfer. From this point forward, we will refer to enhanced GFP (eGFP) as "GFP" and eGFP chromophore[1] as "chromophore" that is the result of the F64L and S65T mutations from the *Aequorea victoria* wild type GFP (wtGFP)[2].

A. Chromophore

Fluorescence in all GFPs begins with the absorption of a photon by the chromophore, typically in the blue region of the visible spectrum (~300 to 500 nm). This absorption process is intimately linked to the unique molecular structure of the chromophore. The chromophore is formed autocatalytically from three amino acid residues—Ser65, Tyr66, and Gly67—through a series of reactions involving cyclization, dehydration, and oxidation. The resulting structure consists of a hydroxybenzylidene imidazolinone moiety, which forms an extended π-conjugated system as shown in Fig. 1. wtGFP chromophore has a primary alchohol group (i.e., Ser) instead of secondary (i.e., Thr).

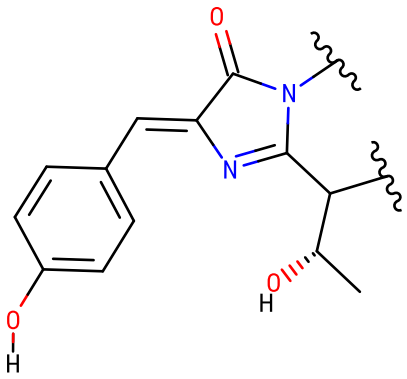

Fig. 1: Neutral (i.e., A state) GFP chromophore.

a. *Excitation:*

The π-conjugated system is a cornerstone of the chromophore's light-absorbing properties. Photons of specific energies, precisely corresponding to the energy gap between the ground state (S_0) and the first excited state (S_1) of the chromophore, excite the delocalized electrons in the conjugated bonds. Planarity, protonation state, and notably the protein environment, collectively contribute to the fine-tuning of the exact absorption wavelength.

When a blue photon is absorbed, it promotes an electron from the highest occupied molecular orbital (HOMO) to the lowest unoccupied molecular orbital (LUMO) of the chromophore. This electronic transition is predominantly $\pi \rightarrow \pi^*$ in nature, reflecting the excitation within the π-conjugated system.

Following absorption, the excited chromophore undergoes rapid vibrational relaxation within the S_1 state, typically on a femtosecond to picosecond timescale. This relaxation involves small structural adjustments in the chromophore and its immediate protein environment, preparing the system for the subsequent fluorescence emission.

b. *Protonation states:*

The protonation state of the GFP chromophore is a critical determinant of its photophysical properties, playing a crucial role in the protein's spectral characteristics and fluorescence behavior. The chromophore can exist in two primary forms: a neutral (protonated) state and an anionic (deprotonated) state, each exhibiting distinct spectroscopic signatures.

In its neutral form (shown in Fig. 1), the chromophore's phenolic oxygen is protonated, resulting in an absorption maximum typically around 395-400 nm. This state is often referred to as the A state. The neutral chromophore generally exhibits weaker fluorescence compared to its anionic

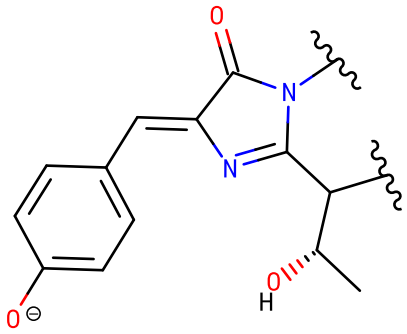

Fig. 2: Anionic (i.e., B state) GFP chromophore.

counterpart, with emission maxima around 460 nm. The reduced fluorescence efficiency of the neutral form is attributed to excited-state dynamics that favor non-radiative decay pathways.

The anionic form of the chromophore, where the phenolic oxygen is deprotonated, is primarily responsible for the characteristic green fluorescence of GFP.

This state, often called the B state, has an absorption maximum at approximately 475-490 nm and emits strongly at around 510 nm. The anionic chromophore demonstrates a higher fluorescence quantum yield, making it the predominant contributor to GFP's bright fluorescence.

The relative population of these two states is influenced by several factors, including the local pH, specific interactions within the protein environment, and mutations in the protein sequence. In wild-type GFP, the chromophore exists in an equilibrium between these two states, with the population distribution heavily dependent on pH. Under physiological conditions, the anionic form is typically favored.

c. *Planarity:*

The planarity of the eGFP chromophore plays a pivotal role in determining its fluorescent properties, particularly through enhanced conjugation and increased quantum yield. These factors contribute significantly to the chromophore's spectroscopic characteristics and efficiency.

Enhanced conjugation in a planar chromophore structure is primarily due to the maximized overlap of p-orbitals in the π-conjugated system. This optimal alignment of p-orbitals, perpendicular to the molecular plane, facilitates efficient delocalization of π-electrons across the entire conjugated system. Such extensive electron delocalization has profound effects on the chromophore's electronic structure, most notably in reducing the energy gap between the highest occupied molecular orbital (HOMO) and the lowest unoccupied molecular orbital (LUMO).

Planarity significantly impacts the chromophore's quantum yield by restricting non-radiative decay pathways. In non-planar configurations, rotation around single bonds, can serve as an efficient route for non-radiative decay. However, when the chromophore is held in a planar conformation by the protein environment, these rotational movements are severely limited. This restriction of molecular motion creates energy barriers in the excited state potential energy surface, effectively preventing the chromophore from accessing geometries that favor non-radiative decay.

Furthermore, the planar structure reduces coupling between electronic and vibrational states, which might otherwise lead to non-radiative relaxation through internal conversion. The minimized structural changes between ground and excited states in a planar chromophore also contribute to reduced internal conversion rates. Consequently, with fewer available non-radiative pathways, the excited chromophore is more likely to return to the ground state via fluorescence emission, directly increasing the fluorescence quantum yield.

d. *Neutral-state fluorescence:*

Excitation and subsequent emission of the neutral state of the chromophore without any structural changes is one—infrequent—possibility.

Excitation of the neutral state occurs at approximately 395 nm, corresponding to the absorption of violet-blue light. This excitation promotes the chromophore to its first excited singlet state (S_1) without immediate proton transfer. The subsequent emission from this excited neutral state results in weak blue fluorescence with a peak around 460 nm.

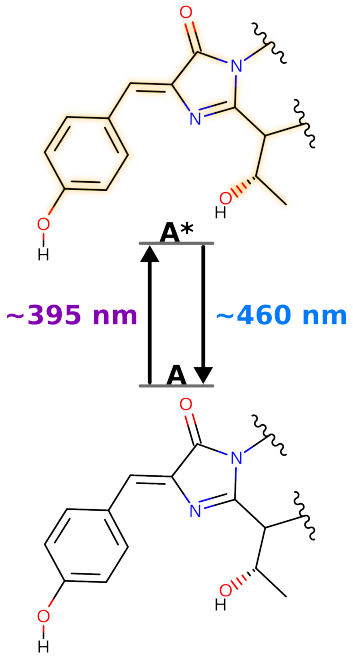

Fig. 3: Excitation and emission of neutral chromophore.

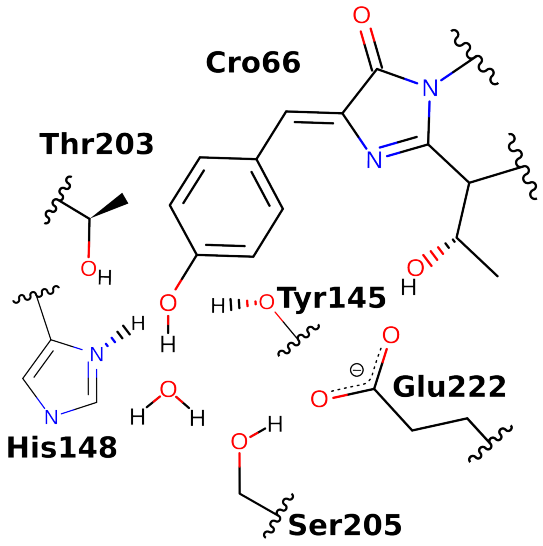

Fig. 4: Example stabalizing configuration for the neutral chromophore.

This protonated chromophore can be further stabilized by hydrogen bonding with a water molecule, Thr203, or Ser205. The presence or absence of these interactions contribute to the distinct excitation and emission. Although, this emission is relatively weak compared to the anionic state discussed next.

e. *Anionic-state fluorescence*:

The anionic state of the chromophore represents a key configuration responsible for the protein's characteristic green fluorescence. In this state, the chromophore exists in its deprotonated form, with the phenolic oxygen carrying a negative charge.

Excitation of the anionic chromophore occurs at approximately 475 nm, corresponding to the absorption of blue light. This excitation promotes the chromophore to its first excited singlet state (S_1). The subsequent relaxation and emission result in the bright green fluorescence typically associated with GFP, with a peak around 508 nm.

The anionic state is stabilized by specific interactions within the protein barrel. Notably, Thr203 plays a crucial role in stabilizing the anionic form through hydrogen bonding with the deprotonated phenolic oxygen. Additionally, a protonated Glu222 could form a hydrogen bond with the anionic chromophore, further contributing to its stabilization.

The protein environment around the chromophore is critical in maintaining this anionic configuration. The β-barrel structure of eGFP provides a hydrophobic pocket that shields the chromophore from bulk solvent, contributing to the high quantum yield of fluorescence in this state.

f. *Excited-state proton transfer:*

The excited-state proton transfer (ESPT) mechanism represents a fundamental process in GFP, contributing significantly to its unique spectroscopic properties. This

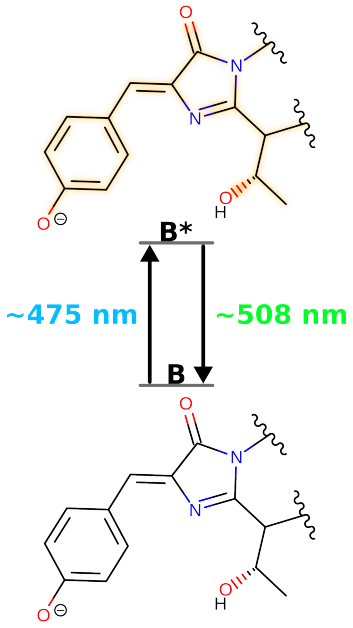

Fig. 5: **TODO:** Add caption

process involves the initial excitation of the neutral (protonated) chromophore, followed by rapid, successive proton transfer events in the excited state, ultimately resulting in emission from an anionic species. An overview of the process is shown below.

1. Upon absorption of a photon at approximately 395 nm, the neutral chromophore is promoted to its first excited singlet state (S_1).
2. In this excited state, the chromophore exhibits markedly different acid-base properties compared to its ground state, becoming a much stronger acid. This enhanced acidity facilitates the transfer of a proton from the chromophore

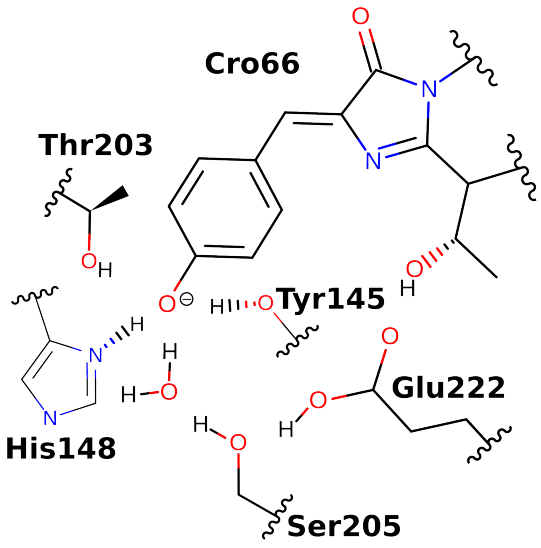

Fig. 6: Example stabalizing configuration for the anionic chromophore.

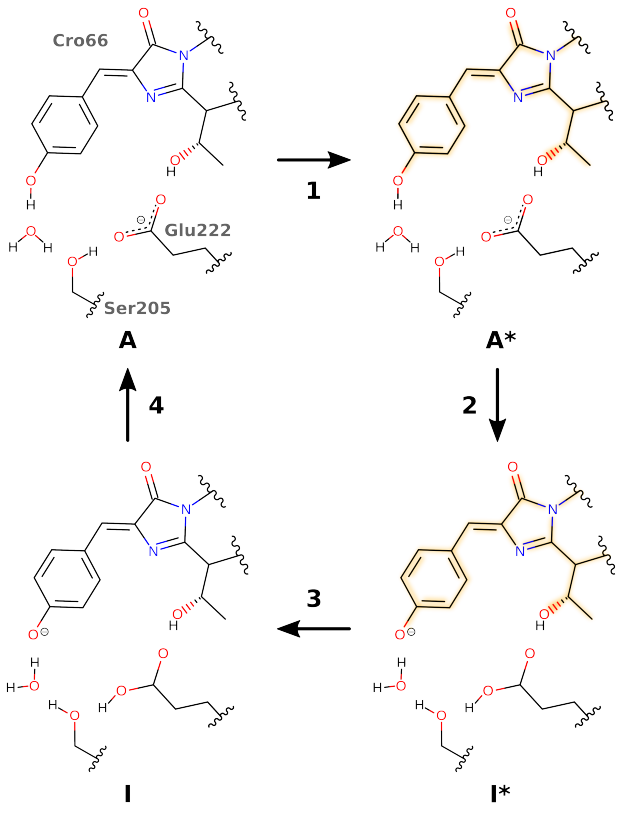

Fig. 7: **TODO: Add caption**

to a proximal acceptor within the protein matrix. The proton transfer pathway involves a sophisticated hydrogen-bonding network. A critical component of this network is a strategically positioned water molecule, which acts as the initial proton acceptor. This water molecule is part of a proton wire that includes Ser205 and terminates at Glu222. The transfer occurs on an ultrafast timescale, typically in the order of picoseconds.

3. Following the ESPT, the system exists transiently in an intermediate state (I*), characterized by an anionic chromophore and a protonated Glu222. I* subsequently relaxes and emits fluorescence at approximately 508 nm, closely resembling the emission profile of the intrinsically anionic chromophore.

4. The final step is a reverse ground-state proton transfer from Glu222 through Ser205, a water molecule, and terminated at the chromophore.

B. Roles of other crucial residues

The exceptional fluorescent properties of GFP arise from a complex interplay of molecular interactions within its β-barrel structure.

a. *His148:*

Structurally, His148 helps maintain β-strand stability by hydrogen bonding to Arg168's backbone **(CITE)**. Others have also explored introducing a hole in the β barrel through an H148G mutation, allowing metal ions to diffuse into the protein and interact directly with the chromophore[3].

His148 directly interacts with the chromophore, forming a critical hydrogen bond. Specifically, the imidazole side chain of His148 donates a hydrogen bond to the chromophore's phenolate oxygen **(CITE)**. This interaction aids in locking the chromophore into a planar conformation. These residues' rigid environment minimizes non-radiative decay pathways, contributing to GFP's high fluorescence quantum yield. =Upon chromophore excitation, His148 also helps facilitates proton movement[4].

b. *Thr203:*

Thr203 is located close to the chromophore within the β-barrel structure. Its hydroxyl group can hydrogen bond with the anionic chromophore's phenolate oxygen in specific conformations. Mutating Thr203 to Ile or Val destabilizes the B-state and dramatically reduces its excitation peak, thus driving the grand-state equilibrium towards the A-state[5]. Yellow FP (YFP) is also derived from mutations by placing chemical groups that can $\pi-\pi$-stacking with the chromophore[6]. Quenching of A* emissions through an ESPT is still present in T203 mutants; however, T203I and T203V mutants are slower down while T203Y maintains wild-type speeds[7].

c. *Tyr145:*

Tyrosine's hydroxyl group produces a bulge in the β-barrel, and a phenylalanine mutation enhances the protein's thermal stability[8]. This mutation alleviates local structural strain, thereby increasing the thermal resilience of the GFP without disrupting its overall β-barrel fold[9].

2. roGFP2 contains redox-sensing cysteines

Redox-sensitive green fluorescent proteins (roGFPs) are engineered variants of GFP designed to report cellular redox states through changes in their fluorescence properties[10]. Among these, roGFP2 has emerged as a particularly useful probe due to its ratiometric readout and midpoint potential, which are suitable for measuring redox conditions in reducing cellular compartments like the cytosol and mitochondria.

roGFP2 contains two cysteine residues (S147C and Q204C) on adjacent β-strands near the chromophore of a GFP variant already containing mutations C48S, S65T, and Q80R. (A structural depiction of the relevant residues is in Fig. 8.) The strategically placed cysteines can form a reversible disulfide bond in response to the surrounding redox environment changes. Formation of this disulfide alters the protonation state of the chromophore, resulting in reciprocal changes in the excitation peaks at 400 nm and 490 nm.

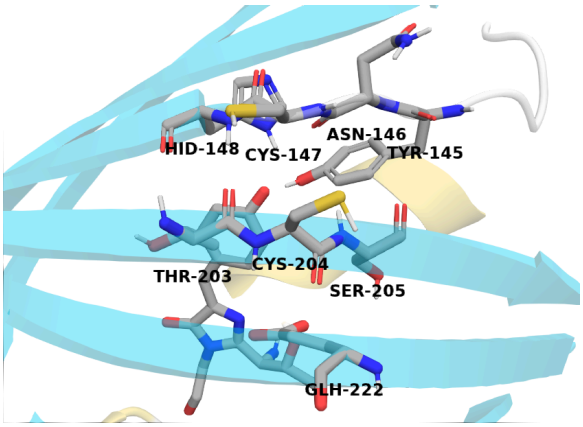

Fig. 8: Fluorescence-relevant residues in reduced roGFP2.

3. roGFP2 fluorescence response

Fig. 9 illustrates the redox-dependent fluorescence properties of roGFP2, showing the protein's excitation spectra under various redox conditions. These spectra were obtained by monitoring emission at 511 nm while scanning excitation wavelengths from 350 to 500 nm. The protein samples were equilibrated in buffers containing different ratios of oxidized and reduced dithiothreitol (DTT) to achieve a range of defined redox potentials.

roGFP2 exhibits two distinct excitation peaks: (1) the A band at 400 nm and (2) the B band at 490 nm. These peaks correspond to 511 nm fluorescence of the chromophore's excited neutral (protonated) and anionic (deprotonated) forms. We will refer to the neutral and anionic forms of the chromophore as "A state" and "B state", respectively.

We observe a clear shift in the excitation spectrum as the environment becomes more oxidizing (moving from −0.240 V to −0.310 V). The intensity of the A band increases significantly, while the B band experiences a concomitant decrease. This spectral shift reflects the formation of the disulfide bond between Cys147 and Cys204 and an increasing preference for the protonated chromophore.

Notably, the spectra display a clear isosbestic point at approximately 425 nm, where the fluorescence intensity remains constant regardless of the redox state. This isosbestic point is a hallmark of a two-state system, confirming that roGFP2 is transitioning cleanly between its oxidized and reduced forms without significant intermediate states. This spectral feature is a critical indicator of the probe's behavior: it suggests that the engineered disulfide bond is forming and breaking as intended, without competing side reactions or alternative conformations significantly affecting the fluorescence. The maintenance of this isosbestic point across various redox potentials implies that the structural changes induced by oxidation and reduction are consistent and

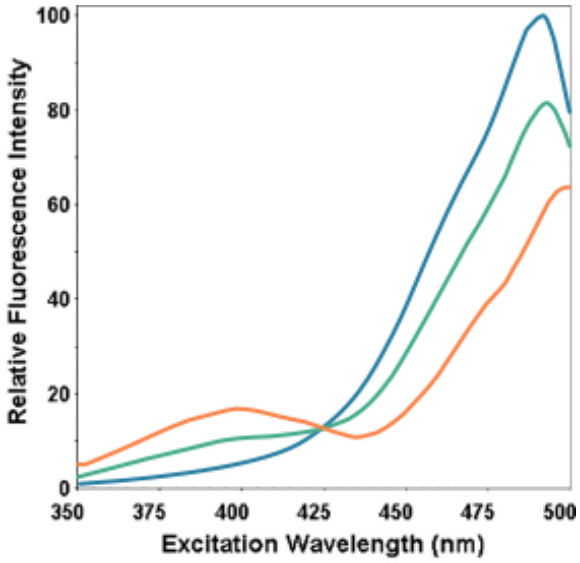

Fig. 9: Relative fluorescence at 511 nm after excitation scan from 350 to 500 nm at −0.310 (blue), −0.275 (green), and −0.240 V (orange) redox potentials. Adapted with permission from Hanson et al.[10] distributed under the CC-BY-4.0 license.

reversible. Any deviation from this behavior, such as a shift in the isosbestic point or its disappearance, would suggest more complex interactions—potentially involving intermediate states, protein structural changes, or interactions with other molecules —that could complicate data interpretation.

A. Possible perturbations

Changes in A- or B-band absorption could indicate a variety of environmental changes in the chromophore.

- **Equilibrium ratio of A or B state populations.** Changes in neutral (A state) or anionic (B state) chromophore stability impacts the relative proportion of A- and B-band absorbance. For example, roGFP1 has a higher A band instead of B band[10]. A-state stability is directly correlated to A-band fluorescence; whereas the B band would be inversely correlated.
- **Excited-state proton transfer (ESPT) from A* → I*.** Emissions at the typical 511 nm (green) fluorescence from the A state requires an ESPT from Cro66 to Glu222 through a coordinated water molecule and Ser205. Prohibiting ESPT would result in radiative emission at 460 nm which often is not monitored experimentally.
- **Ground-state proton transfer (GSPT) from I → A.** Reprotonating the chromophore through a GSPT is crucial for maintaining the A band and B-band lifetime. Disrupting the Glu222 → Ser205, Ser205 → H_2O, or H_2O → Cro66 pathway would decrease the A-state population—likely with a corresponding B state increase.
- **Non-radiative emissions.** Enahnced flexibility of the chromophore through protein conformational shifts would

lead to additional non-adiabatic crossings; thereby lowering the relative fluorescence in that state.

4. Molecular simulations

A. *Protein preparation*

Initial protein structures for reduced (1JC0) and oxidized (1JC1) states of roGFP2 were retrieved from the Protein Data Bank (PDB). The structures were processed using in-house Python and bash scripts (available free of charge at gitlab.com/oasci/studies/metalflare). The first chain, along with the crystallographic water molecules, were centered to the origin while minimize the box values using NumPy **(CITE)**, SciPy **(CITE)**, and MDAnalysis **(CITE)** packages.

Given the relevance and availability of the GFP mechanism's force field parameters, the chromophore was modeled in its anionic state. All selenomethionine residues (MSE) were converted to methionine (MET), and Cys147 and Cys204 were transformed into the appropriate residues. Glu222 was protonated to model the I state of the GFP photocycle; this still probes the anionic chromophore's stability while offering insight into GSPT dynamics. The protonation states of all other residues were determined with PDB2PQR[11], using the default parameters to ensure standardization. The pdb4amber tool was then used to validate the PDB file before proceeding.

B. *Cu(I) placement*

TODO: Add GFN2-xTB calculations.

C. *Simulation preparation*

System preparation was performed using the tleap module of AmberTools v23.6 **(CITE)**. The protein structure was parameterized using the ff19SB force field **(CITE)**. For the solvent environment, we employed the OPC3 water model, **(CITE)**, which is known for its balanced representation of water properties in biomolecular simulations. The 12-6 nonbonded model and parameters for all ions were taken from Sengupta et al[12]. The system was neutralized by adding Na+ and Cl- ions as needed. Additional ions were introduced to achieve a solvent ionic strength of 0.150 M to mimic physiological conditions. The protein was solvated in a rectangular box, with a minimum distance of 10 Å between the protein and the box edges to minimize periodic boundary condition artifacts. Parameters from Breyfogle et al.[13] were employed for the anionic chromophore.

D. *Minimization*

The prepared system underwent a four-stage energy minimization protocol using Amber23 **(CITE)** to relieve any unfavorable interactions and optimize the structure. All minimization stages used the steepest descent method for the first 1000 steps, followed by the conjugate gradient method for the remaining steps, with a maximum of 5000 steps per stage. A non-bonded cutoff of 10.0 Å was applied throughout. Periodic boundary conditions were employed, and coordinates were wrapped to the primary unit cell. The minimization progress was monitored by writing energies every step and coordinates every 200 steps.

Stage 1: Initial minimization was performed with restraints (force constant: 5.0 kcal/mol/Å²) on all non-hydrogen atoms of the entire system, allowing hydrogen atoms to relax and adjust their positions. *Stage 2:* The system was further minimized with restraints (force constant: 5.0 kcal/mol/Å²) on all non-hydrogen atoms of the solute (excluding water molecules and ions), allowing solvent and ions to equilibrate around the solute. *Stage 3:* Minimization continued with reduced restraints (force constant: 2.0 kcal/mol/Å²) applied only to the protein backbone, allowing side chains and other flexible parts to relax. *Stage 4:* Final minimization was performed with further reduced restraints (force constant: 1.0 kcal/mol/Å²). The resulting minimized structure served as the starting point for subsequent relaxation and production simulations.

E. *Relaxation simulations*

Following energy minimization, the system underwent a three-stage relaxation protocol using Amber23 to gradually equilibrate the structure and solvent. Three independent runs were initiated with random initial velocities to ensure adequate sampling. All subsequent simulations were continued using the respective run's restart files.

Stage 1: An initial 20 ps NVT (constant Number of particles, Volume, and Temperature) simulation was performed with a 2 fs time step. The system was heated from 100 K to 300 K using Langevin dynamics with a collision frequency of 5 ps^{-1}. Restraints (force constant: 1.0 kcal/mol/Å²) were applied to the protein backbone. SHAKE algorithm was used to constrain bonds involving hydrogen atoms. The non-bonded cutoff was set to 10.0 Å. *Stage 2:* A 1 ns NPT simulation followed, maintaining the temperature at 300 K using Langevin dynamics (collision frequency: 5 ps^{-1}). Pressure was regulated at 1.01325 bar using the Monte Carlo barostat with a relaxation time of 1 ps. Restraints on the same atoms were reduced (force constant: 0.5 kcal/mol/Å²). *Stage 3:* The final relaxation stage consisted of a 1 ns NPT simulation with all positional restraints removed.

F. *Production simulations*

All production runs were performed under the same setup as the last relaxation stage. Each run was simulated for 500 ns with coordinates saved every ten ps. The resulting trajectories from all three replicates were used for subsequent analyses, providing a cumulative 1.5 μs of simulation data for the system under study.

G. *Analysis*

From the MD trajectories, we extracted two primary sets of data:

1. Dihedral angles (φ, ψ) were calculated using MDAnalysis **(CITE)** for specific residues known to be crucial for roGFP2 function.
2. Key interactions between various residues through intermolecular distances.

Dihedral angles were transformed using

$$\frac{1 - \cos(\theta)}{2}$$

This transformation maps the circular dihedral data to a [0, 1] range, preserving the periodicity while differentiating between cis and trans conformations.

All input features (X) were standardized using sklearn's $\mathrm{StandardScaler}$ to ensure each feature contributes equally to the model. This transformation ensures continuity across the periodic boundary, facilitating more accurate modeling.

a. *Coordinated water detection:*

TODO: Write this.

b. *Potential of mean force (PMF):*

TODO: Write this.

c. *Feature correlation:*

To investigate the relationship between structural descriptors and various features, we employed Partial Least Squares (PLS) regression analysis. This multivariate statistical technique was chosen for its ability to handle high-dimensional, correlated data and reveal underlying patterns in complex datasets.

A PLS regression model was fitted to X and response variable y using sklearn's $\mathrm{PLSRegression}$ with two components for each simulation state. The model's performance was evaluated using the R^2 score.

Data points were projected onto the space of the first two PLS components. A 2D histogram was created in this space, with bin colors representing the mean y.

Loading vectors for each feature were plotted as arrows in the PLS component space. The magnitude and direction of these arrows indicate the importance and relationship of each feature to the PLS components. The magnitude of each feature's loading vector was calculated as the Euclidean norm of its first two PLS components.

A dashed line representing the direction of maximum change in the response variable was added to the plot. This line, referred to as the derivative line, indicates the direction in the PLS component space along which y increases most rapidly.

H. *Feature importance*

We developed a machine learning pipeline to elucidate the relationship between backbone dihedral angles and the target feature. Our approach employed two complementary models:

- **XGBoost Regressor:** A gradient boosting algorithm chosen for its high performance and ability to capture non-linear relationships **(CITE)**.
- **Elastic Net:** A regularized linear regression model selected to identify linear correlations while mitigating multicollinearity **(CITE)**.

The dataset was randomly partitioned into training (80%) and testing (20%) sets, ensuring model generalizability. We utilized $\mathrm{GridSearchCV}$ with 3-fold cross-validation to tune model hyperparameters. For XGBoost, we optimized the number of estimators (250-700), learning rate (0.05-0.2), maximum tree depth (5-9), and regularization terms (α: 0.0-0.2, γ: 0.8-1.0). For Elastic Net, we tuned the regularization strength (α: 10^{-5} - 5) and L1 ratio (0.2-1.0). Performance was assessed using mean squared error (MSE) and coefficient of determination (R^2) on the held-out test set.

Feature Importance Analysis We extracted XGBoost feature importance scores directly from the model, but used absolute values of the ElasticNet coefficients as a proxy for feature importance. This dual-model approach allows for a robust comparison of feature rankings, mitigating model-specific biases.

I. *Hydrogen bond cutoff*

A hydrogen bond of X—H ··· Y—Z, where X is the donor and Y is the acceptor atom, can be classified based on distances and angles. One characteristic recommended by IUPAC is that the H ··· Y distance is less than the sum of H and Y van der Waals radii. Hydrogen (1.10 Å) and oxygen (1.52 Å)[14] would have a cutoff of 2.62 Å. Others[15] recommend a cutoff of 2.50 Å based on structural analysis[16] and quantum chemical calculations[17]. Since the difference between a 2.5 and 2.62 Å cutoff is likely a substantially weak hydrogen bond, we will use a H ··· Y cutoff of 2.5 Å.

5. Fluorescence mechanism of Cu(I) distinct from oxidation

Joel Rosenbaum performed in vitro assays of roGFP2 under H_2O_2 (i.e., oxidation) and Cu(I) conditions by monitoring 528 nm emissions **TODO: Check emission value** with scanning excitation wavelengths between 380 and 500 nm. Relative fluorescence with respect to **TODO: How was this normalized? Check methods** is shown in Fig. 10.

Apo represents our control with roGFP2 in its reduced state. Adding 1.0 mM H_2O_2 results in the expected shift in the A- and B-band proportions. Again, this indicates that oxidizing Cys147

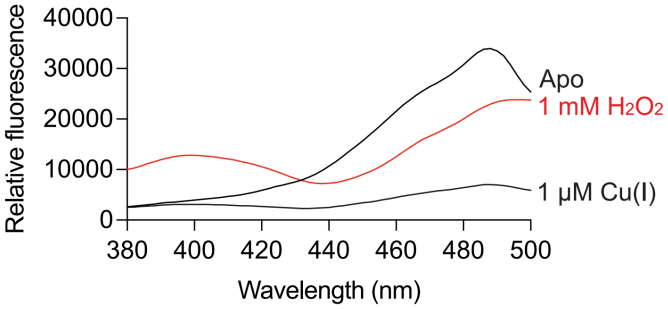

Fig. 10: Relative fluorescence of roGFP2 under reduced, oxidized, and Cu(I) conditions from 380 to 500 nm excitation scan. **TODO: Check emission value?** Apo (i.e., reduced) roGFP2 exhibits typical bimodal absorption of A-band (excited at 400 nm) and B-band (excited at 488) peaks. Upon roGFP2 oxidation from 1 mM H_2O_2, a shift in A- (increased) and B-band (decreased) absorption and subsequent 528 nm emission marks a corresponding change in neutral and anionic chromophore populations. Binding of Cu(I), however, exhibits a larger decrease in B-band without the A-band increase observed when oxidized.

and Cys204 and forming a disulfide bridge increases the neutral chromophore equilibrium proportion—with a corresponding decrease in the anionic state. This oxidation-induced change in the chromophore protonation state is the basis for roGFP2's utility as a redox sensor in biological systems.

Cu(I), on the other hand, exhibits an entirely different fluorescence response. Strikingly, a mere 1 μM of Cu(I) drastically reduces the B-band intensity while keeping the A band relatively stable. The distinct responses to oxidation and Cu(I) binding provide compelling evidence that Cu(I) binding to roGFP2 does not simply alter the chromophore's protonation state preference, as oxidation does. Instead, these results suggest that Cu(I) may disturb the anionic chromophore's electronic state or induce conformational changes that specifically affect its environment, underscoring the need for further exploration.

6. Cu(I) binding enhances roGFP2 backbone flexibility

First, we investigate the backbone dynamics over 1.5 μs of MD simulations.

A. *Cys147 and Cys207 C_α distance*

Experimental structures of both the reduced (PDB ID: 1JC0) and oxidized (PDB ID: 1JC1) states of for roGFP2 exhibited a mean C_α-C_α distance of 4.30 ± 0.12 and 4.07 ± 0.09 Å, respectively[10]. Our MD simulations agreed well with experimental observations as shown in Table I with mean differences less than 0.04 Å.

Table I: Mean and standard deviations of C_α-C_α distances between Cys147 and Cys204.

State	Experimental (Å)	Simulations (Å)
Reduced	4.30 ± 0.12	4.34 ± 0.47
Oxidized	4.07 ± 0.09	4.11 ± 0.29
Cu(I)	N/A	4.78 ± 0.82

The standard deviations, σ, also provide an indication of conformational flexibility. Unsurprisingly, the σ of oxidized roGFP2 exhibits is substantially smaller than the reduced state.

An experimental structure of roGFP2-Cu(I) is currently not available; however, our simulations suggest that it is on average 0.44 Å larger than the reduced state. Cu(I) stayed coordinated between Cys147 and Cys204 throughout all simulations while enhancing conformational flexibility. For example, Fig. 11 shows a broader distribution of C_α-C_α distances with a slight bimodal peaks centered around 4.48 Å and 4.96 Å.

B. *β-strand fraying*

GFP and its variants are characterized by a distinctive β-barrel structure, which plays a crucial role in their fluorescence properties. This β-barrel is composed of 11 β-strands, forming a robust scaffolding that encapsulates and protects the centrally located chromophore. The structural integrity of this β-barrel is essential for maintaining the protein's fluorescence characteristics and its sensitivity to environmental changes. In roGFP2, Cys147 is strategically positioned near the C-terminus of a β-pleated sheet, flanked by His148 and Thr203 (Figure Fig. 8).

Our molecular dynamics simulations reveal a striking structural change upon Cu(I) binding to roGFP2. Specifically, we observe a significant disruption in the β-sheet structure near Cys147. Fig. 12 illustrates that Cu(I) binding leads to the

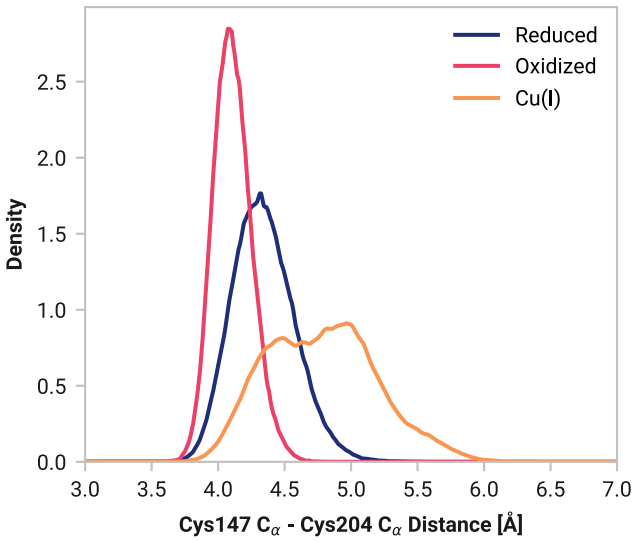

Fig. 11: **TODO: Add caption**

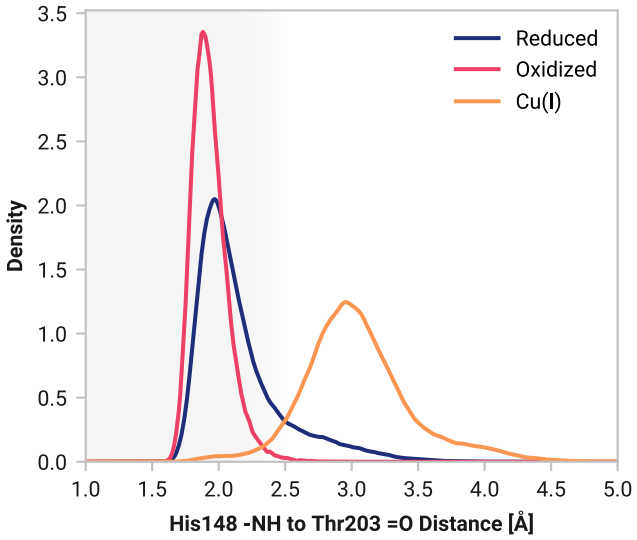

Fig. 12: Probability density of His148 and Thr203 backbone hydrogen bonding under various roGFP2 conditions.

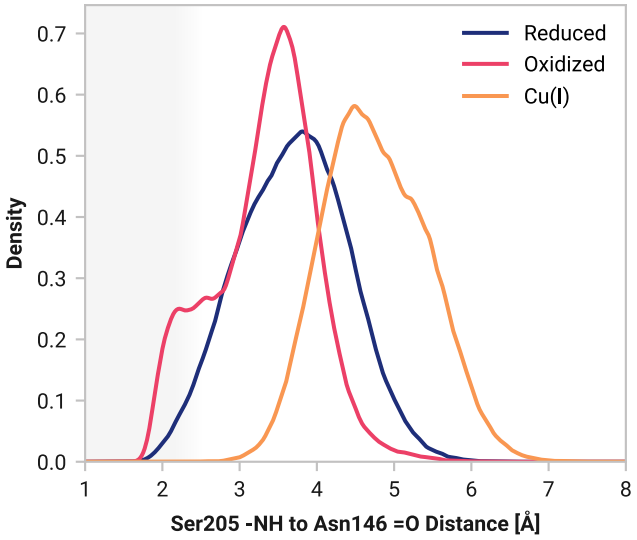

Fig. 13: **TODO:** Add caption

breaking of a key β-sheet hydrogen bond in this region. This observation is further substantiated by quantitative analysis presented in Table II, which shows a dramatic decrease in the hydrogen bond probability between the backbone –NH and C=O groups within a 2.5 Å distance. The probability drops from 0.865 in the reduced state to a mere 0.063 in the Cu(I)-bound state, indicating a near-complete loss of this stabilizing interaction. (Unsurprisingly, oxidized roGFP2 stabilizes this hydrogen bond.)

This disruption of the β-sheet hydrogen bonding network can be characterized as "fraying" of the β-strand. Fraying is a phenomenon where the regular hydrogen bonding pattern at the termini of secondary structure elements, particularly β-strands, becomes disrupted, leading to increased local flexibility.

In the case of roGFP2, the Cu(I)-induced fraying at the C-terminus of this β-strand is likely to have several important implications. Given the proximity of this structural change to the chromophore, it may directly influence the chromophore's electronic environment, contributing to the observed changes in fluorescence properties upon Cu(I) binding.

The structural perturbation at this site could also propagate through the protein structure. Indeed, Fig. 13 shows the intermolecular distance peak between Asn146 and Ser205 increasing from 3.80 to 4.48 Å with bound Cu(I). Distances with Cu(I) extends out to at least 0.66 Å further than the reduced state. Under oxidizing conditions, the peak distance only decreases to 3.56 Å and hydrogen bonds 14.4 % during the course of the simulations.

No changes are observed in the Val150 and Leu201 β-strand.

Table II: Hydrogen bonding probability between residue backbones

State	His148 - Thr203	Asn146 - Ser205
Reduced	0.865	0.047
Oxidized	0.997	0.144
Cu(I)	0.063	0.000

7. Cu(I) binding affects anionic chromophore hydrogen binding

As previously mentioned, several residues are in close proximity to the chromophore. Numerous studies have observed complex interactions and have led to several variants tailord for specific applications. roGFP2 is no different.

A. His148 and Tyr145

Our analysis of hydrogen bonding interactions with the chromophore in roGFP2 revealed distinct patterns across different protein states. Fig. 14 illustrates the 2D potential energy surfaces for Tyr145 and His148 interactions with the chromophore.

In the reduced state of roGFP2, we observed a diverse energy landscape characterized by multiple local minima. A minimum is located at Tyr145-chromophore and His148-chromophore distances of approximately 1.8 Å and 1.85 Å respectively. This minimum corresponds to a configuration where both residues simultaneously form hydrogen bonds with the chromophore. Two other local minima were observed, representing configurations where either Tyr145 or His148 independently formed a hydrogen bond with the chromophore. Still, both residues exhibit conformational flexibility where neither residues stabilize the anionic chromophore. This pattern suggests significant conformational flexibility in the reduced state, allowing for various hydrogen bonding arrangements.

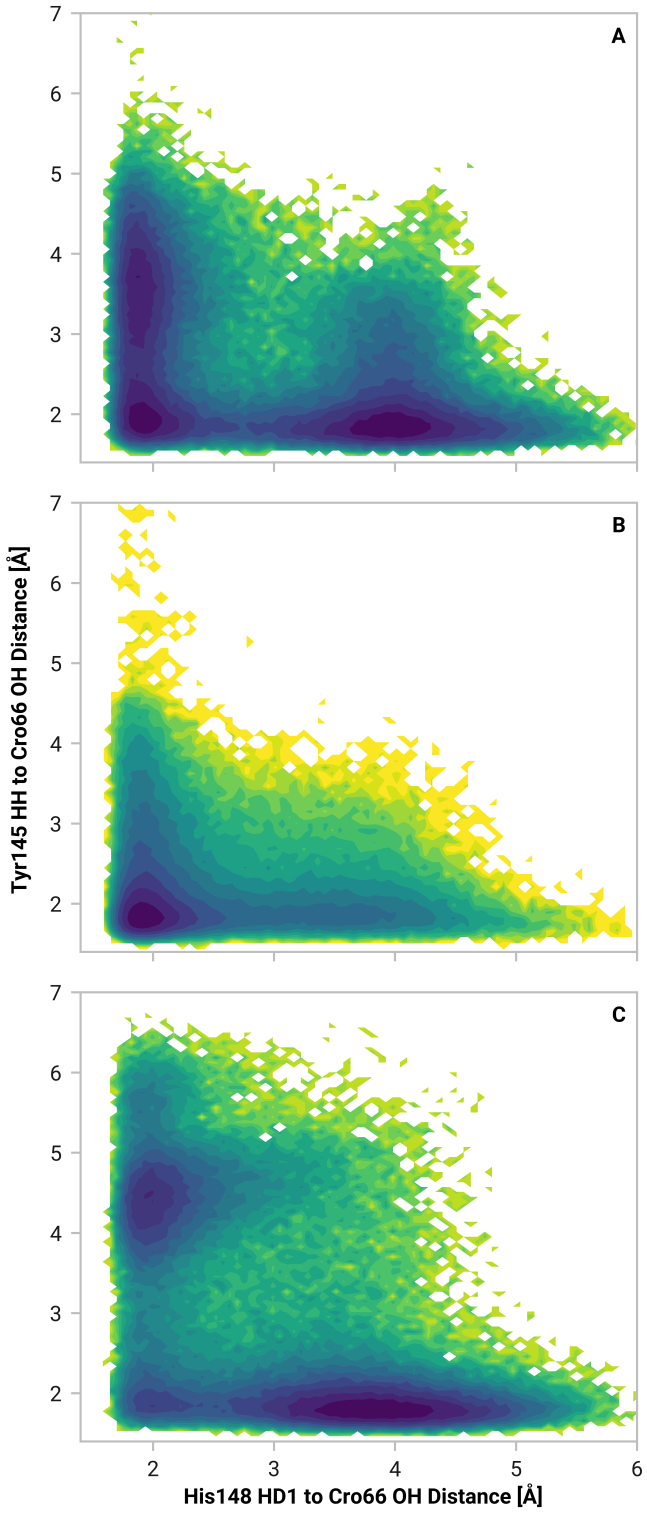

Fig. 14: **TODO:** Add caption

Upon oxidation of roGFP2, we noted a marked change in the energy landscape. The oxidized state exhibited a single, pronounced global minimum at similar Tyr145-chromophore (1.80 Å) and His148-chromophore (1.91 Å) distances as the reduced state. However, this energy well was deeper and narrower than the reduced state. The absence of significant additional local minima indicates a strong preference for the configuration where both Tyr145 and His148 simultaneously hydrogen bond with the chromophore. This suggests that oxidation induces a more rigid and stable arrangement of these critical residues around the chromophore.

Table III: Structural hydrogen bonding probability to chromophore

State	Thr203	His148	Tyr145	Glu222
Reduced	0.191	0.486	0.612	0.689
Oxidized	0.009	0.691	0.795	0.977
Cu(I)	0.619	0.339	0.641	0.895

By contrast, the Cu(I)-bound state of roGFP2 exhibited similar minima as reduced simulations but with a notable increase in flexibility with shallower minima. The dual-hydrogen bonding minimum was significantly less pronounced than the reduced and oxidized states. It is worth noting that Tyr145 is 1.9 times more likely to hydrogen bond to the chromophore compared to His148, indicating an asymmetry in their hydrogen bonding behavior.

His148 and Thr203 β-strand fraying appears to correlates correlate with decreased stabilization of the anionic chromophore through His148. **TODO:** Add origin analysis

B. *Thr203*

Our molecular dynamics simulations reveal a striking change in the hydrogen bonding behavior of Thr203. In the reduced state of roGFP2, we observe several distribution peaks of Thr203-chromophore distances. Two primary peaks at 5.32 and 1.75 Å suggest dynamic populations across the simulations.

Oxidation of roGFP2 dramatically alters this interaction. The hydrogen bonding population decreases substantially, with a minor peak at 1.80 Å. Instead, we observe a dominant peak at

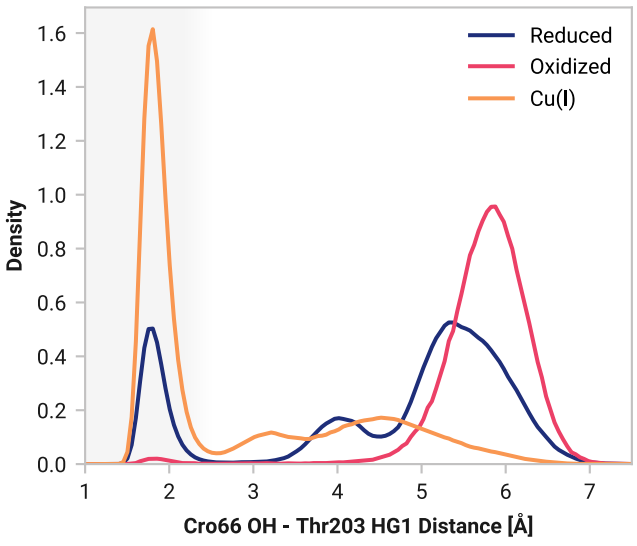

Fig. 15: **TODO:** Add caption

TABLE IV: GSPT STEP PROBABILITY

State	Glu222 → Ser205	Ser205 → H_2O	H_2O → Cro66
Reduced	0.299	0.516	0.465
Oxidized	0.000	0.416	0.379
Cu(I)	0.000	0.517	0.452

5.83 Å, indicating that oxidation largely disrupts the Thr203-chromophore hydrogen bond. This disruption likely contributes to the shift in chromophore protonation state observed upon oxidation.

Remarkably, Cu(I) binding to roGFP2 significantly enhances the Thr203-chromophore hydrogen bond. We observe a sharp, dominant peak at 1.75 Å, which is more than three times the corresponding peak in the reduced state. This dramatic increase in hydrogen bonding suggests that Cu(I) binding induces a conformational change that positions Thr203 optimally for interaction with the chromophore.

8. Disruption of ground-state proton transfer

9. Proposed Cu(I) fluorescence mechanism

TODO: writeeee

References

(1) Cormack, B. P. ; Valdivia, R. H. ; Falkow, S. FACS-Optimized Mutants of the Green Fluorescent Protein (GFP). *Gene* **1996**, *173* (1), 33–38

(2) Prasher, D. C. ; Eckenrode, V. K. ; Ward, W. W. ; Prendergast, F. G. ; Cormier, M. J. Primary Structure of the Aequorea Victoria Green-Fluorescent Protein. *Gene* **1992**, *111* (2), 229–233

(3) Barondeau, D. P. ; Kassmann, C. J. ; Tainer, J. A. ; Getzoff, E. D. Structural Chemistry of a Green Fluorescent Protein Zn Biosensor. *Journal of the American Chemical Society* **2002**, *124* (14), 3522–3524

(4) Shinobu, A. ; Palm, G. J. ; Schierbeek, A. J. ; Agmon, N. Visualizing Proton Antenna in a High-Resolution Green Fluorescent Protein Structure. *Journal of the American Chemical Society* **2010**, *132* (32), 11093–11102

(5) Kummer, A. D. ; Wiehler, J. ; Rehaber, H. ; Kompa, C. ; Steipe, B. ; Michel-Beyerle, M. E. Effects of Threonine 203 Replacements on Excited-State Dynamics and Fluorescence Properties of the Green Fluorescent Protein (GFP). *The Journal of Physical Chemistry B* **2000**, *104* (19), 4791–4798

(6) Zimmer, M. Green Fluorescent Protein (GFP): Applications, Structure, And Related Photophysical Behavior. *Chemical reviews* **2002**, *102* (3), 759–782

(7) Jung, G. ; Wiehler, J. ; Zumbusch, A. The Photophysics of Green Fluorescent Protein: Influence of the Key Amino Acids at Positions 65, 203, And 222. *Biophysical journal* **2005**, *88* (3), 1932–1947

(8) Nasu, Y. ; Shen, Y. ; Kramer, L. ; Campbell, R. E. Structure- and Mechanism-Guided Design of Single Fluorescent Protein-Based Biosensors. *Nature chemical biology* **2021**, *17* (5), 509–518

(9) Akiyama, S. ; Suenaga, A. ; Kobayashi, T. ; Kamioka, T. ; Taiji, M. ; Kuroda, Y. Experimental Identification and Theoretical Analysis of a Thermally Stabilized Green Fluorescent Protein Variant. *Biochemistry* **2012**, 7974–7982. https://doi.org/10.1021/bi300580j

(10) Hanson, G. T. ; Aggeler, R. ; Oglesbee, D. ; Cannon, M. ; Capaldi, R. A. ; Tsien, R. Y. ; Remington, S. J. Investigating Mitochondrial Redox Potential with Redox-Sensitive Green Fluorescent Protein Indicators. *Journal of Biological Chemistry* **2004**, *279* (13), 13044–13053. https://doi.org/10.1074/jbc.m312846200

(11) Jurrus, E. ; Engel, D. ; Star, K. ; Monson, K. ; Brandi, J. ; Felberg, L. E. ; Brookes, D. H. ; Wilson, L. ; Chen, J. ; Liles, K. ; others. Improvements to the APBS Biomolecular Solvation Software Suite. *Protein Science* **2018**, *27* (1), 112–128

(12) Sengupta, A. ; Li, Z. ; Song, L. F. ; Li, P. ; Merz Jr, K. M. Parameterization of Monovalent Ions for the Opc3,

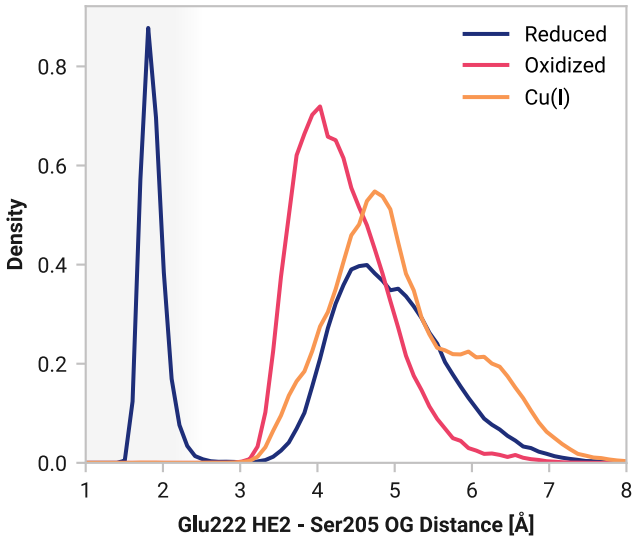

Fig. 16: **TODO:** Add caption

OPC, Tip3p-FB, And Tip4p-FB Water Models. *Journal of chemical information and modeling* **2021**, *61* (2), 869–880

(13) Breyfogle, K. L. ; Blood, D. L. ; Rosnik, A. M. ; Krueger, B. P. Molecular Dynamics Force Field Parameters for the EGFP Chromophore and Some of Its Analogues. *The Journal of Physical Chemistry B* **2023**, *127* (26), 5772–5788. https://doi.org/10.1021/acs.jpcb.3c01486

(14) Mantina, M. ; Chamberlin, A. C. ; Valero, R. ; Cramer, C. J. ; Truhlar, D. G. Consistent Van Der Waals Radii for the Whole Main Group. *Journal of Physical Chemistry A* **2009**, *113* (19), 5806–5812

(15) Hubbard, R. E. ; Haider, M. K. Hydrogen Bonds in Proteins: Role and Strength. *Encyclopedia of life sciences* **2010**, *1*, 1–6

(16) McDonald, I. K. ; Thornton, J. M. Satisfying Hydrogen Bonding Potential in Proteins. *Journal of molecular biology* **1994**, *238* (5), 777–793

(17) Liu, Z. ; Wang, G. ; Li, Z. ; Wang, R. Geometrical Preferences of the Hydrogen Bonds on Protein- Ligand Binding Interface Derived from Statistical Surveys and Quantum Mechanics Calculations. *Journal of Chemical Theory and Computation* **2008**, *4* (11), 1959–1973